Transmit Frequency Adaptation for Contrast to Tissue Ratio Optimization in Second Harmonic Imaging

Sébastien Ménigot, Jean-Marc Girault

Transmit Frequency Adaptation for Contrast to Tissue Ratio Optimization in Second Harmonic Imaging

Sébastien Ménigot [1,2,*], Jean-Marc Girault [1,2,†]

[1] Université François-Rabelais de Tours, UMR-S930, Tours, France.
[2] Inserm, U 930, Tours, France.

[*] sebastien.menigot@univ-tours.fr, [†] jean-marc.girault@univ-tours.fr

Published in:
Journal of Electrical and Control Engineering
2012 Vol.2 No.5 pp.9-14
http://www.joece.org/paperInfo.aspx?ID=115

***Abstract*—Conventional ultrasound contrast imaging systems use sequences of sine waves at a fixed transmit frequency. The excitation of the system is thus a sine wave whose frequency is often fixed around two-thirds of the center frequency of the transducer in the second harmonic imaging. However, this choice requires a knowledge of the transducer and does not take into account the specificities of microbubbles and medium. The main purpose of our study was to propose an automatic technique providing the best contrast-to-tissue ratio by selecting the optimal transmit frequency. The simulations and the experiment showed that the optimal transmit frequency value did not correspond to the usual value. By using the optimized value, the contrast was improved by around 6 dB. Finally, by providing a closed loop system, the system automatically proposed the optimal control without any a priori knowledge of the system or the medium explored.**

***Index Terms*—Adaptive system, closed loop system, contrast enhancement, microbubbles, optimal control, optimization, second harmonic, signal processing, transmitted pulse, ultrasound imaging.**

I. Introduction

Over the past twenty years, research in medical ultrasound imaging systems have enabled to improve the image quality in terms of sensitivity, contrast and resolution. To provide additional qualitative information about physiology and pathology [1], clinicians have used intravenous injection of ultrasound contrast agents containing microbubbles. These microbubbles can generate harmonic components of the transmitted ultrasound wave explained from the equations of nonlinear dynamics of the microbubble [2]. Moreover, these harmonic components generated by the microbubbles are more intense than those generated by soft tissues when the pressure level of the transmitted wave is small [3]. The contrast is thus enhanced by increasing the contrast-to-tissue ratio (*CTR*) and particularly the harmonic power P_b backscattered by the microbubbles compared to the harmonic power P_t backscattered by the tissue [4]:

$$CTR\,(2f) = \frac{P_b(2f)}{P_t(2f)} \tag{1}$$

where f is the transmit central frequency.

However, obtaining an ideal imaging method has been limited by two factors. Firstly, a good separation of the harmonic components requires a limited pulse bandwidth [5], which reduces the axial resolution as in the second harmonic imaging [6]. Secondly, the effects of the ultrasound wave propagation limit the *CTR*. Several imaging methods have been proposed to improve the contrast. Some techniques are based on post-processings such as second harmonic imaging [6], subharmonic imaging [7], super harmonic imaging [8], imaging using second order Volterra filter [4] and attenuation correction [9]. Other techniques are based on discrete or continuous encoding of amplitude, phase or frequency of the ultrasound wave transmitted such as pulse inversion [10], power modulation [11], contrast pulse sequencing [12], pulse subtraction [13] and har-

monic chirp imaging [3], [14]. Since the easiest and the most commonly used technique is the second harmonic imaging, we focused our study on this technique. The optimal use of such technique is only ensured if the setting parameters, *e.g.* the transmit frequency, is adjusted to its optimal value. However, this optimal setting is not assured in commercial devices to date, since the solution of our problem often requires inaccessible *a priori* knowledge of the medium and the transducer. Consequently, the transmit frequency was only set to the two-thirds of the transducer central frequency [15] from empirical inference. Thus the question that we can naturally ask is: is there a choice of a transmit frequency which maximizes the criterion of contrast as the *CTR*?

In this study, we aimed to solve this problem through the concept of the optimal command: the transmit frequency f was set by optimizing *CTR* in second harmonic imaging:

$$f^\star = \arg\max_f \left(\mathit{CTR}(f) \right), \tag{2}$$

where $f^\star$ is the optimal transmit frequency which provides the best *CTR*. Therefore we replaced the current system with a closed loop system whose transmitted pulse was modified by feedback. We proposed an iterative approach to find the optimal transmit frequency $f^\star$ and we tested the originality of our solution both by simulation and experiment.

II. Open loop Imaging System

As previously mentioned, the studied imaging system was a second harmonic imaging system [6]. The principle of this system was described in Fig. 1. It consists of transmitting an incident ultrasound wave of frequency f to the medium, and then receiving the harmonic component generated by the medium at the frequency $2f$. The contrast is thus enhanced by improving the microbubble detection compared to the tissue. Note that the bandwidth of the transducer was shared by the two filters (emission and reception filters).

The pulse signal $x_k(t)$ at transmit frequency f_k was computed digitally with Matlab (Mathworks, Natick, MA, USA):

$$x_k(t) = A \cdot w_k(t). \tag{3}$$

Note that in the case of the open loop system, the iteration was always the same with $k = 1$.

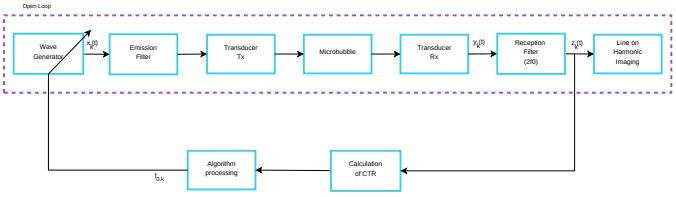

Fig. 1. Block diagram of adaptive second harmonic imaging

The Gaussian-modulated sinusoidal pulse [14] $w_k(t)$ was constructed as follows:

$$w_k(t) = \exp\left[-\frac{(t-t_0)^2}{\frac{N_c}{2f_k}} \right] \sin(2\pi f_k), \tag{4}$$

where t is the time, t_0 the time for which the Gaussian function is maximum and N_c the cycle number. The value of N_c must be significant enough in order to limit the transmitted bandwidth. In this case, direct transmissions at the harmonic frequencies could be avoided and thus measured the harmonic components provided by a nonlinear behavior [5].

Finally, the power P_w of the transmitted signal was equal to the power $P_{x_{ref}}$ of the reference signal defined to the two-thirds of the central frequency $2/3f_c$ of the transducer and with a driving pressure A_0. The amplitude of the driving pressure A was thus adjusted as follows:

$$A = \sqrt{\frac{A_0^2 \cdot P_{x_{ref}}}{P_w}}. \tag{5}$$

At the receiver, the backscattered signal $y_k(t)$ was filtered by the transducer and by the reception filter at the frequency $2f$. The final signal $z_k(t)$ represented a line of the second harmonic image.

CTR_k was then computed from the line $z_k(t)$. However, in order to compute the powers P_b and P_t in eq. 1, the area of the microbubbles and the area of the tissue were determined manually before the optimization process.

III. Closed loop Imaging System

The closed loop system was composed of the open loop system and a feedback. This feedback ensures the optimization of the cost function, which is here the *CTR* in the second harmonic imaging (eq. 2). This cost function was mainly based on the upcoming hypotheses. It must:

- depend on the transmit frequency f;

- be, in absolute, independent of the simulation model or the experiment;
- be concave in the range of the transmit frequency f to increase the robustness of the algorithm.

A. Iterative Optimization Algorithm

Based on the last hypotheses, a simple algorithm can be based on the principle of the gradient descent [16]. It determined a new transmit frequency f_{k+1} at the iteration $k+1$ for the next pulse sequence to optimize the CTR_{k+1} according to the following recurrence relation:

$$f_{k+1} = f_k + \mu_k \cdot d_k, \tag{6}$$

The first coefficient μ_k set the speed of convergence as follows:

$$\mu_k = \begin{cases} 0 & \text{if } k \leqslant 3; \\ \Delta f & \text{if } k = 4; \\ \mu_{k-1} & \text{if } \operatorname{sgn}(\nabla CTR(f_k)) = \operatorname{sgn}(\nabla CTR(f_{k-1})); \\ \frac{\mu_{k-1}}{2} & \text{if } \operatorname{sgn}(\nabla CTR(f_k)) \neq \operatorname{sgn}(\nabla CTR(f_{k-1})). \end{cases} \tag{7}$$

where Δf was fixed at 100 kHz providing the best compromise between the speed of the convergence and the robustness, the sign function $\operatorname{sgn}(t)$ is equal to 1 if $t > 0$, 0 if $t = 0$ and -1 if $t < 0$, and the *CTR* gradient defined by:

$$\nabla CTR(f_k) = \frac{CTR_k - CTR_{k-1}}{f_k - f_{k-1}}. \tag{8}$$

where $f^\star$ is the optimal transmit frequency. The second coefficient d_k set the direction as follows:

$$d_k = \begin{cases} 1 & \text{if } k \leqslant 3; \\ 1 & \text{if } \operatorname{sgn}(\nabla CTR(f_k)) = \operatorname{sgn}(\nabla CTR(f_{k-1})); \\ -1 & \text{if } \operatorname{sgn}(\nabla CTR(f_k)) \neq \operatorname{sgn}(\nabla CTR(f_{k-1})). \end{cases} \tag{9}$$

In order to compute μ_k and d_k, the system operated in open loop for the first three iterations ($k = \{1, 2, 3\}$). The first three frequencies f_1, f_2 and f_3 were chosen initially. The appropriate choice could increase the speed of convergence, but it was not essential to reach the optimal *CTR*, when the cost function was concave.

B. Gain

Finally, the contrast gain G_{dB} was defined between the optimized system and the non-optimized system. The *CTR* obtained with the non-optimized system was determined at the two-thirds of the central frequency $2/3f_c$ of the transducer [15]. The contrast gain G_{dB} was obtained by the following equation:

$$G_{dB} = \frac{CTR(f^\star)}{CTR(2/3f_c)}. \tag{10}$$

IV. Simulation Evaluation

The optimization principle was initially applied in simulation. Several simulations were performed to demonstrate the feasibility of our new method.

A. Simulation Model

The simulation model followed the same process as in the experimental setup (Fig. 1). A pulse signal was digitally generated at the iteration k and filtered by the emission filter at 2.25 MHz with a fractional bandwidth of 74% at -3 dB. It was then transmitted simultaneously in microbubble and tissue models to deduce the surface pressures. In reception, the signal measured by the transducer was filtered around 3.5 MHz with a fractional bandwidth of 63% at -3 dB. Note that the transducer was centred at $f_c = 3$ MHz and with a fraction bandwidth of 160% at -3 dB.

1) Microbubbles:

The simulated ultrasound contrast agent had the properties of encapsulated microbubbles of SonoVue (Bracco Research SpA, Geneva, Switzerland). The microbubble gas was composed of a phospholipid monolayer imprisoning sulfur hexafluoride gas (SF_6) [17]. The mechanical shell properties were the shear modulus G_s 46 MPa [18] and the resonance frequency of the microbubble was 2.1 MHz [19].

To carry out the simulations, the free simulation program BUBBLESIM by Hoff [20] was used to calculate the oscillations and the scattered echoes for a specified contrast agent and excitation pulse. A modified version of the Rayleigh-Plesset model was chosen. The model was based on the theoretical description of microbubbles as air-filled particles with surface layers of elastic solids presented by Church [21] and later modified by Hoff [20]. The properties of the surrounding medium were those of blood, since the microbubble is supposed to be moving in the vascular system. In order to simulate the mean behavior of a microbubble cloud, we

hypothesized that the response of a cloud of N microbubbles was N times the response of a single microbubble with the mean properties.

2) Tissue:

The tissue response was simulated by fat globules with a density of 928 kg/m^3 [22]. The computation of their response was based on Rayleigh backscattering [23] for a small fat ball of 10 μm, the size that was chosen to approximate the small size of fat cells. We hypothesized that the response of N particles was N times the response of a single particle.

B. Simulation Results

1) Empirical Optimization:

Fig. 2 represents the results of the first simulation, *i.e.* the *CTR* as a function of the transmit frequency for different pressure levels A_0 (240 and 370 kPa) and for 4 cycles.

The first result indicated that the *CTR* had a global maximum whatever the pressure level A_0. These maxima were obtained neither with the two-thirds of the central frequency of the transducer, nor with the microbubble resonance frequency. This result showed that the *CTR* can be improved by choosing the appropriate transmit frequency, thus confirming the validity of our study. Secondly, the global maximum was the single maximum in the studied range. This property was interesting, because an automatic search could be achieved more easily by a gradient algorithm. Thirdly, the maximum values of the *CTR* ranged between 17.4 dB and 20.5 dB for pressure levels A_0 240 and 370 kPa, and the contrast gain G_{dB} ranged from 5 to 5.9 dB.

To summarize, the results shown in Fig. 2 confirmed the need to optimize the imaging system by seeking the best transmit frequency which maximized the *CTR* function. Indeed, Fig. 2 shows that the *CTR* depended on transmit frequency f and could reach a single global maximum of approximately 20 dB. The single maximum of the *CTR* could be detected automatically by a simple technique such as the gradient.

2) Automatic Optimization:

The maximum *CTR* was reached automatically using the gradient algorithm. Fig. 3b shows the *CTR* measured at each iteration k, and Fig. 3a shows variations in the transmit frequency during iterations.

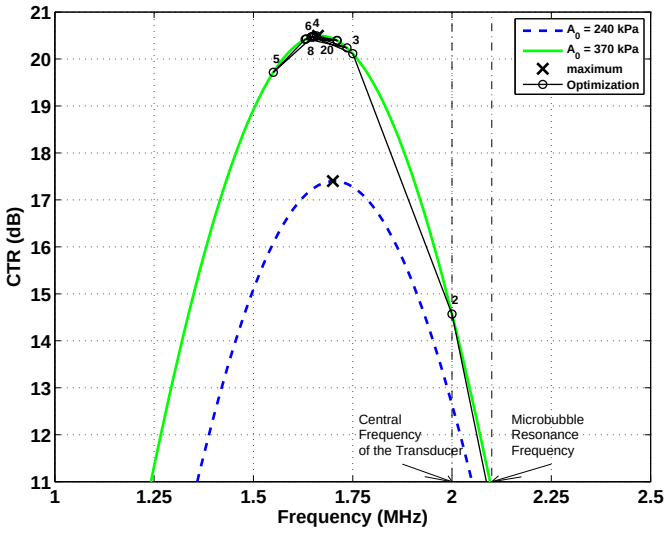

Fig. 2. Simulation of *CTR* for a transmit frequency of 1 to 2.5 MHz, a pressure level A_0 of 240 and 370 kPa and a constant number of cycles N_c of 4. The simulation included the transducer

The transmit frequency converged to a stable value after six iterations, whatever the pressure level A_0. As an illustration, the black solid line in Fig. 2 shows the first twenty iterations which confirmed the convergence after the first six iterations. Moreover, the *CTR* reached its maximum when the transmit frequency converged. Note that the *CTR* and the contrast gain G_{dB} obtained automatically were equal to those obtained empirically in the first simulation.

In summary, the results in Fig. 3 showed that it was possible to find the transmit frequency which maximized the *CTR* automatically. No *a priori* knowledge was required, except for the choice of the first three transmit frequencies which impacted on the speed of convergence.

V. Experimental Validation

The aim of this section was to confirm experimentally the results obtained in simulation.

A. Experimental Setup

The experimental setup was presented in Fig. 1. The transmitted signal was firstly generated digitally by a personal computer using equation 3. It was sent to the medium via a transducer. The wave insonified the medium which was composed of tissues and microbubbles. The receiver collected the echo $y_k(t)$ and computed a second harmonic image line.

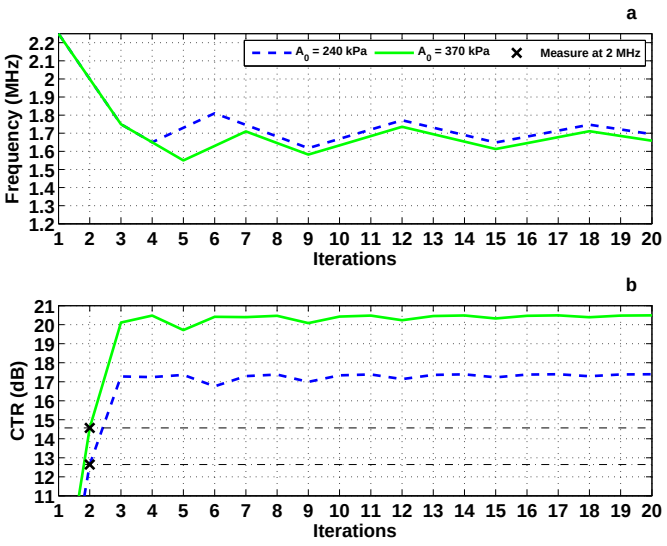

Fig. 3. Simulation of automatic optimization of the *CTR* by iterative searching for the optimal transmit frequency for different pressure levels A_0 of 240 and 370 kPa and a constant cycle number N_c of 4. The simulation included the transducer

1) Measurements and Transducers:

The pulse was chosen with a cycle number N_c of 4 and with a pressure level A_0 of 370 kPa at the focal point. This transmitted signal $x_k(t)$ was transmitted through a GPIB port (National Instruments, Austin, TX) to an arbitrary function generator (33220A, Agilent, Palo Alto, CA). The signal was then amplified using a power amplifier (Amplifier Research 150A100B, Souderton, PA) and transmitted to a 2.25 MHz PZT single element transducer (Sofranel, Sartrouville, France) focused at 55 mm and with a fractional bandwidth of 74%.

The backscattered signals were measured by a 3.5 MHz PZT single element transducer with a fractional bandwidth of 63%, placed perpendicularly to the transmitter, also focused at 55 mm and used in the receiver mode. Note that this setup configuration can look upon as a single transducer centred at $f_c = 3$ MHz and with a bandwidth of 160% at -3 dB.

The echoes measured were amplified by 30 dB (Pulser-Receivers 5072R, Olympus Panametrics, Waltham, MA, USA) and then visualized on a digital oscilloscope (Tektronix, Beaverton, OR). Signals were transferred to a personal computer through a GPIB port for further analysis.

2) Medium Explored:

The wave propagated through a blood mimicking fluid ("EU-DFS-BMF-ver.1.2", Dansk Fantom Service, Jyllinge, Denmark). This latter was crossed by a 1cm-side tank in which there was a $1/2000$ diluted solution of Sonovue™ microbubbles.

B. Experimental Results

The experimental results presented in Fig. 4 showed the transmit frequency and the *CTR* during the iterations. The *CTR* converged to its optimal value after six iterations for a transmit frequency of 1.2 MHz. The mean *CTR* achieved after convergence was around 11.7 dB, *i.e.* a mean contrast gain of 6.8 dB.

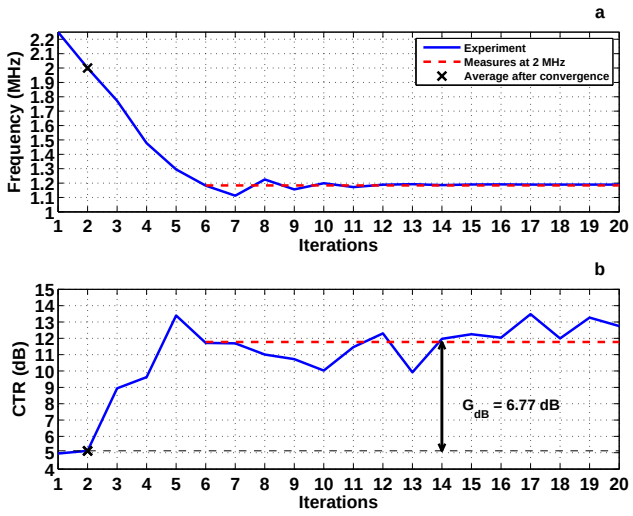

Fig. 4. Experiment of *CTR* optimization for a pressure level A_0 of 370 kPa at the focal length and a constant cycle number N_c of 4

Our simulation was in accordance with the experimental results: we observed that the optimal transmit frequency was lower than the central frequency of the transducer. Furthermore, this optimal transmit frequency obtained after the algorithm convergence also made it possible to receive the second harmonic component required in the *CTR* optimization.

Although the *CTR* was time-varying due to the non-stationarity of the contrast agents, these experimental results confirmed the feasibility of our method. Note that there was a difference between the *CTR* value in our simulation and the one obtained in our experiment. This difference might be due to the simplified hypotheses of the model.

VI. Discussion and Conclusions

CTR optimization in second harmonic imaging was performed automatically by estimating the

transmit frequency f. This optimization was obtained through the imaging system without taking into account *a priori* knowledge of the medium or the transducer, except for the first three values of the transmit frequency chosen only for their impact on the speed of convergence. The optimal transmit frequency was reached automatically by a feedback within only a few iterations.

CTR had a single maximum in simulation. An easily implemented algorithm based on gradient was thus robust. Although this property was demonstrated in experiment, the proposed algorithm itself adjusted the transmit frequency to maximize the power backscattered by microbubbles while minimizing the power backscattered by the tissue within the transducer bandwidth.

One major advantage of our approach was its independence of the medium explored since the cost function was exclusively based on the input and the output measurements of our system. One interesting consequence is that our method can be applied to any imaging system.

Note that a real-time implementation was possible, since the computation time was insignificant. However, the method requires a programmable analogue transmitter. Moreover, for an efficient optimization, it is important to determine the correct position of the perfused and non-perfused areas.

To conclude, the method described ensured optimal *CTR* by selecting the transmit frequency. With our new approach, manufacturers and clinicians do not need themselves to tune the transmit frequency. The method automatically adapts the transmit frequency to help the diagnosis improvement.

Our closed-loop method can be adapted using a larger number of contrast imaging techniques. The only remaining difficulty is in the instrumentation. However, the current development of new imaging methods based on chirp or time reversal also requires this instrumentation.

ACKNOWLEDGEMENTS

The authors thank the Agence Nationale de la Recherche (Projects ANR-07-TECSAN-015 MONITHER and ANR-07-TECSAN-023 SURFOETUS) for financial support.

The authors would like to thank A. Zaylaa and A. Novell for helpful discussions and for language editing of the manuscript, and the Clinical Investigation Centre for Innovative Technology of Tours (CIC-IT 806 CHRU de Tours, Tours, France) for the ultrasound contrast agents.

REFERENCES

[1] P. J. A. Frinking, A. Bouakaz, J. Kirkhorn, F. J. Ten Cate, and N. de Jong, "Ultrasound Contrast Imaging: Current and New Potential Methods," *Ultrasound Med. Biol.*, vol. 26, no. 6, pp. 965–975, Jul. 2000.

[2] T. G. Leighton, *The Acoustic Bubble*. London, UK: Academic Press, Jun. 1994.

[3] J. M. G. Borsboom, C. T. Chin, and N. de Jong, "Nonlinear Coded Excitation Method for Ultrasound Contrast Imaging," *Ultrasound in medicine and biology*, vol. 29, no. 2, pp. 277–284, Feb. 2003.

[4] P. Phukpattaranont and E. S. Ebbini, "Post-Beamforming Second-Order Volterra Filter for Pulse-Echo Ultrasonic Imaging," *IEEE Trans. Ultrason., Ferroelectr., Freq. Control*, vol. 50, no. 8, pp. 987–1001, Aug. 2003.

[5] M. A. Averkiou, "Tissue Harmonic Imaging," in *Proc. IEEE Ultrason. Symp.*, vol. 2, 2000, pp. 1563–1572.

[6] P. N. Burns, "Instrumentation for Contrast Echocardiography," *Echocardiography*, vol. 19, no. 3, pp. 241–258, Apr. 2002.

[7] F. Forsberg, W. T. Shi, and B. B. Goldberg, "Subharmonic Imaging of Contrast Agents," *Ultrasonics*, vol. 38, no. 1-8, pp. 93–98, Mar. 2000.

[8] A. Bouakaz, S. Frigstad, F. J. Ten Cate, and N. de Jong, "Super Harmonic Imaging: A New Imaging Technique for Improved Contrast Detection," *Ultrasound Med. Biol.*, vol. 28, no. 1, pp. 59–68, Jan. 2002.

[9] M.-X. Tang, J.-M. Mari, P. N. T. Wells, and R. J. Eckersley, "Attenuation Correction in Ultrasound Contrast Agent Imaging: Elementary Theory and Preliminary Experimental Evaluation," *Ultrasound Med. Biol.*, vol. 34, no. 12, pp. 1998–2008, Dec. 2008.

[10] D. H. Simpson, C. T. Chin, and P. N. Burns, "Pulse Inversion Doppler: A New Method for Detecting Nonlinear Echoes from Microbubble Contrast Agents," *IEEE Trans. Ultrason., Ferroelectr., Freq. Control*, vol. 46, no. 2, pp. 372–382, Mar. 1999.

[11] G. A. Brock-fisher, M. D. Poland, and P. G. Rafter, "Means for Increasing Sensitivity in Non-linear Ultrasound Imaging Systems," U.S. Patent 5 577 505, Nov., 1996.

[12] P. Phillips and E. Gardner, "Contrast-Agent Detection and Quantification," *Eur. Radiol.*, vol. 14, pp. 4–10, Oct. 2004.

[13] J. M. G. Borsboom, A. Bouakaz, and N. de Jong, "Pulse Subtraction Time Delay Imaging Method for Ultrasound Contrast Agent Detection," *IEEE Trans. Ultrason., Ferroelectr., Freq. Control*, vol. 56, no. 6, pp. 1151–1158, Jun. 2009.

[14] J. M. G. Borsboom, C. T. Chin, A. Bouakaz, M. Versluis, and N. de Jong, "Harmonic Chirp Imaging Method for Ultrasound Contrast Agent," *IEEE Trans. Ultrason., Ferroelectr., Freq. Control*, vol. 52, no. 2, pp. 241–249, Feb. 2005.

[15] J. A. Hossack, P. Mauchamp, and L. Ratsimandresey, "A High Bandwidth Transducer Optimized for Harmonic Imaging," in *Proc. IEEE Ultrason. Symp.*, vol. 2, 2000, pp. 1021–1024.

[16] B. Widrow and S. Stearns, *Adaptive Signal Processing*. Englewood Cliffs, New Jersey, USA: Prentice Hall, 1985.

[17] C. Greis, "Technology Overview: SonoVue (Bracco, Milan)," *Eur. Radiol. Suppl.*, vol. 14, no. 8, pp. 11–15, Oct. 2004.

[18] H. J. Vos, F. Guidi, E. Boni, and P. Tortoli, "Method for Microbubble Characterization Using Primary Radiation Force," *IEEE Trans. Ultrason., Ferroelectr., Freq. Control*, vol. 54, no. 7, pp. 1333–1345, Jul. 2007.

[19] S. Ménigot, A. Novell, A. Bouakaz, and J.-M. Girault, "Improvement of the Power Response in Contrast Imaging with Transmit Frequency Optimization," in *Proc. IEEE Ultrason. Symp.*, 2009, pp. 1–4.
[20] L. Hoff, *Acoustic Characterization of Contrast Agents for Medical Ultrasound Imaging*. Boston, USA: Kluwer Academic, 2001, ch. 3, pp. 158–160.
[21] C. C. Church, "The Effects of an Elastic Solid Surface Layer on the Radial Pulsations of Gas Bubbles," *J. Acoust. Soc. Am.*, vol. 97, no. 3, pp. 1510–1521, Mar. 1995.
[22] T. Szabo, *Diagnostic Ultrasound Imaging: Inside Out*. Oxford, UK: Academic Press, 2004.
[23] J. W. S. Rayleigh, *The Theory of Sound*. Macmillan, 1896, vol. 2, ch. 15, pp. 149–154.

Sébastien Ménigot was born in France in 1985. He received his M. Sc. degree in medical imaging technology from François Rabelais University of Tours, France, in 2008. He obtained his Ph. D. degree in signal processing in medical ultrasound imaging at François Rabelais University of Tours, France, in 2011. His research focuses on optimal control applied to ultrasound imaging systems.

Jean-Marc Girault received the Master's degree in "signal processing and biological and medical imaging" from the University of Angers, France, in 1996. He obtained his Ph. D. degree in signal processing in medical ultrasound imaging at François Rabelais University of Tours, France, in 1999. Finally, he obtained his "Habilitation Diriger les Recherches" (HDR) in signal processing in medical ultrasound imaging at François Rabelais University of Tours, France, in 2010. He has been a lecturer in signal processing at the University of Tours since 2001. He has written more than fifty scientific communications on medical ultrasound imaging and signal processing. Since 2005 he has been the coordinator of the Master's Degree in "medical imaging" at University François Rabelais of Tours. At the same time, he coordinates the cross-discipline group focusing on "signals, images, imaging" at UMR Inserm-CNRS-University François Rabelais of Tours S930 entitled "Imaging and Brain".